VERSITA

Central European Journal of Chemistry
DOI: 10.2478/s11532-007-0053-5
Research article
CEJC 5(4) 2007 931–950

Characterization of the passive films on electrodeposited Fe-Ni-Cr alloys in borate solution at pH 8.4

Laura Sziráki[1*], Ernő Kuzmann[2†], Colin U. Chisholm[3‡], Mahmoud R. El-Sharif[3], Lilla Bóbics[1], Sándor Stichleutner[4]

[1] *Department of Physical Chemistry of Eötvös Loránd University*

[2] *Hungarian Academy of Sciences, Eötvös Loránd University 1518 Budapest P.O.B. 32, Hungary*

[3] *Glasgow Caledonian University Glasgow G4 0BA, Scotland, United Kingdom*

[4] *Institute of Isotopes, Hungarian Academy of Sciences, Budapest, Hungary*

Received 17 July 2007; accepted 24 September 2007

Abstract: The corrosion properties of the passive layers formed on iron-nickel-chromium electrodeposits of $Fe_{29}Ni_{51}Cr_{20}$ were investigated in 0.3 M borate solution at a‘ pH of 8.4. On the basis of measurements by cyclic voltammetry, chronopotentiometry and electrochemical impedance spectroscopy, a low passive dissolution/corrosion rate was identified for the electrodeposited Fe-Ni-Cr alloys due to the nature of the established corrosion layer. The stability of this passive layer was further enhanced after corrosion under oxidizing conditions. Mössbauer spectroscopic measurements confirmed the existence of a thin passive layer on the amorphous electrodeposits.

Keywords: passive film, microcrystalline alloy, surface modification, electrochemical impedance, conversion electron Mössbauer spectroscopy.

1 Introduction

Fe-Ni-Cr alloys have a very wide area of application within modern technology. One of the possible potential developments of Fe-Ni-Cr alloy films is related to the preparation of high temperature superconductor wires. These “second generation” of superconductors, used

* sziraki@chem.elte.hu
† kuzmann@chem.elte.hu
‡ c.chisholm@gcal.ac.uk

for the transmission of electricity are based on work reported earlier on the suitability of substrates such as nickel and nickel alloys [1]. These alloys are textured and then usually coated with a ceramic buffer layer. In addition to the existence of the texture there is a requirement for the formation of a thin passive layer on the surface of the substrate metal. The role of the ceramic buffer layer is to protect the metal substrate during the heat treatment procedures and to provide a better adjustment to the lattice parameters of the superconductor. A superconducting film is then applied to the metal – ceramic composite leading to the establishment of the superconducting tape. The thermal stability of the metallic substrate as well as the mechanical properties can be enhanced by alloying the base metal (for this study nickel) with other metals such as chromium and iron to form alloy electrodeposits on the substrate.

On the basis of this information, the aim of this study was to investigate the corrosion properties and the creation of a passive layer formed on the iron-nickel-chromium electrodeposits. ^{57}Fe conversion electron Mössbauer spectroscopy was used to detect and explain the nature of the phase composition of the passive layer. The sensitivity of this analysis was enhanced by enriching the iron isotopically with ^{57}Fe in the electrodeposited Fe-Ni-Cr alloys.

Mössbauer spectroscopy can be used to probe the local electronic density, the electric field gradient as well as the magnetic field and the lattice vibrations at the site of the Mössbauer active element. Therefore, on the basis of the Mössbauer parameters it is possible to differentiate various microenvironments where the Mössbauer probe atom is accommodated. In the case of iron-containing alloys, the authors have previously shown that Mössbauer spectroscopy is sufficiently sensitive to distinguish between ordered or disordered, crystalline or amorphous structures as well as ferromagnetic or paramagnetic states, and therefore can be highly effective to determine both the qualitative and quantitative phase analysis of alloy phases and oxide compounds formed on the surface of alloys [2–4]. On this basis, it was anticipated, that this technique would also be effective in the development of passive films on Ni-Cr-Fe in borate solutions.

The Fe-Ni-Cr electrodeposited films were prepared using trivalent chromium dimethylformamide-water electrolytes with a continuous flow circulation cell process [5] which had previously been shown to give good quality metallic alloy electrodeposits. Further work by the authors [6] using Mössbauer spectroscopy, and x–ray diffraction (XRD) measurements clearly show the electrodeposits from this process to be amorphous/microcrystalline depending on the combination of the deposition parameters as well the dominant phase in the electrodeposit was found to be ferromagnetic. In contrast, the thermally prepared alloys of similar composition consisted only of a paramagnetic phase.

It is well established that the critical passivating current for the different amorphous/microcrystalline alloys is significantly smaller than that for crystalline metals and therefore, it is now generally accepted that the corrosion rate of the amorphous/microcrystalline alloys tends to be small due to the strong tendency to give spontaneous passivation. This was confirmed in our earlier work [7] using alloys of composition $Fe_{50}Ni_{25}Cr_{25}$ passivated in sulphuric acid. However, higher passive current densities have been recorded

for nanocrystalline materials, [8, 9] and this has been attributed by the researchers to either the passive film being more defective or thinner compared to films formed on polycrystalline materials. The authors also noted that enhanced stability of the passive layer against local corrosion has been reported by other researchers for nanocrystalline Fe-Ni-Cr alloys [10, 11].

On the basis of these conflicting results, an investigation was conducted to gain a better understanding of the corrosion characteristics of the passive layers formed on electrodeposited alloys exhibiting amorphous/microcrystalline structures.

The passive layer on the stainless steel surface formed under natural atmospheric or wet corrosion conditions is only a few nm thick and consists mainly of chromium oxides incorporating iron oxides/hydroxides and some nickel oxide. The composition and structure of the passive layer strongly depends on the passivating media and the corrosion or anodic potential. Enhancing the protective nature of the passive layer using different chemical, physical or electrochemical methods is of continual interest for the further development of practical applications of these materials. For example, it has been reported that cycling or pulsing the potential is a commonly used procedure to facilitate the production of thick, porous oxide layers with modified electrochemical properties on stainless steel alloys [12–15]. Chromium, iron or nickel oxide enrichment was observed in the passive film and this was associated with the values of the cathodic and anodic end potentials and other circumstances. The alternate voltage (*av*) treatment carried out on commercial stainless steel between different potential limits in passivating media is aimed at enhancing the protective value of the layer [12]. The alternate voltage passivation reported proved to be significantly more effective than the potentiostatic passivation. However a more effective corrosion protection could be achieved if the *av* procedure was followed by post-treatment in an oxidizing media.

In our work, a passivation procedure using a square-wave potential pulse of 3 Hz (stepping the potential between –0.7 V and 0.3 V vs. saturated calomel electrode (*sce*)) was applied as a possible method for modification of the passive layer to provide an increase in the amount of the iron oxides in the layer. Electrochemical impedance spectroscopy was used to characterize the corrosion films formed by the spontaneous passivation on the surface of the electrodeposited Fe-Ni-Cr alloys. Two corrosion conditions were tested; the first involved corrosion immersion in a de-aerated solution of pH 8.4 and the second involved wet corrosion of the specimen which was then exposed to atmospheric corrosion conditions. The aim was to characterize the effect of the stability of the various corrosion layers.

2 Experimental

The electrodeposited samples were prepared using a continuous flow plating system which was developed and reported earlier [5]. The conditions are described in Table 1. The average composition of the samples was $Fe_{29}Ni_{51}Cr_{20}$. SEM/EDS (scanning electron microscope with energy dispersive spectrometer) micro-analysis was carried out across

the sample surface and showed the fluctuation of the Ni and Cr content to be within 5–10 w%. Iron was isotopically enriched with ^{57}Fe to enhance the sensitivity of the Mössbauer measurements. The specimens were produced with a surface area of 1 cm^2.

Table 1 Parameters of electrodeposition.

Bath constituents / mol · dm^{-3}		Electrodeposition conditions	
$CrCl_3 \cdot 6H_2O$	0.80	Time of deposition	27 min
$NiCl_2 \cdot 6H_2O$	0.20	Electrolyte temperature	20 °C
$^{57}FeCl_2 \cdot 4H_2O$	0.02	Flow rate (circulation cell)	100 cm^3/min
NaCl	0.50	Anode (40x60 mm)	graphite rod
NH_4Cl	0.50	Cathode (25 mm)	copper plate
$B(OH)_3$	0.15	Cathode potential	–1.8 V vs *sce*
H_2O deionized	500g	Bulk pH	1.8
DMF	500g		

Specimen A was obtained from the side, while the specimen B was obtained from the middle of the original electroplated cathodes. The lateral components of the cut samples were isolated with chemically resistant lacquer. A surface area of 0.5 cm^2 from these specimens were exposed to the electrochemical treatments. All parallel samples showed similar electrochemical behaviour.

The passivating media used was 0.3 M Na_3BO_3 at a pH of 8.4, deoxygenated by bubbling argon gas. A *sce* was used as the reference electrode. The solution movement in the main compartment of the three electrode cell was achieved using a magnetic stirrer. Prior to the corrosion/passivation measurements the samples were degreased with acetone in an ultrasonic cleaning apparatus (type Realsonic 40S, power 120 W). The air-formed oxides were removed using cathodic activation as follows: subsequent potential steps of –1.25, –1.3 and –1.4 V were applied for 2 to 5 minutes and each step was repeated 5 times until the reduction currents remained constant. While this electrochemical reduction probably did not result in a totally free surface state, it did give comparable similar conditions for all the parallel samples.

After activation the samples were then immersed in the de-aerated passivating media for 18 h of corrosion testing. In order to increase the passivity of the samples a wet-dry cycle of corrosion exposure was also used which involved 18 h of wet corrosion immersion followed by 18 h of exposure in air at ambient temperature and humidity. After the oxidizing effect of the atmospheric exposure the electrochemical impedance measurements were repeated in a de-aerated solution with a stable corrosion potential. This method ensured that the differences in the corrosion rates for the two types of corrosion layers can be attributed only to the stability of corrosion layers.

The Solartron 1250 FRA and 1286 Electrochemical Interface were used to measure the electrochemical impedance spectra (EIS) at the steady-state corrosion potential established in a de-aerated 0.3 M borate solution. The amplitude of the sine wave potential perturbation was 7 mV *rms*, and the data were recorded in the frequency range between

20 kHz and 5 MHz. To reduce the high frequency impedance distortion, the reference electrode was shunted by a platinum wire with a capacitance of 0.1 μF. The impedance diagrams were validated using the complex nonlinear least squares (CNLS) fitting procedure included in the Zplot (version 2.6, Scribner Associates, Inc.) electrochemical impedance software. The calculation was carried out by data modulus weighting ($|Z|^{-2}$). The standard error of the fit was calculated as, s_r^2 = weighted sum of squares/degrees of freedom. The residuals of the "best fit" models were randomly distributed over the measured data between the 12 kHz and 0.1 Hz frequency range.

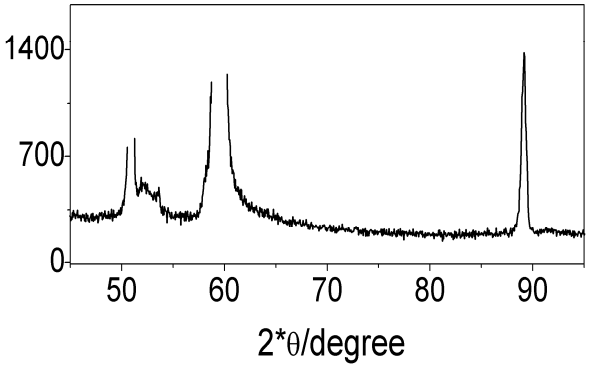

Fig. 1 XRD pattern of $Fe_{29}Ni_{51}Cr_{20}$ electrodeposit. The large peaks represent the Cu substrate since the penetration depth of the X–ray is higher than the thickness of the deposit.

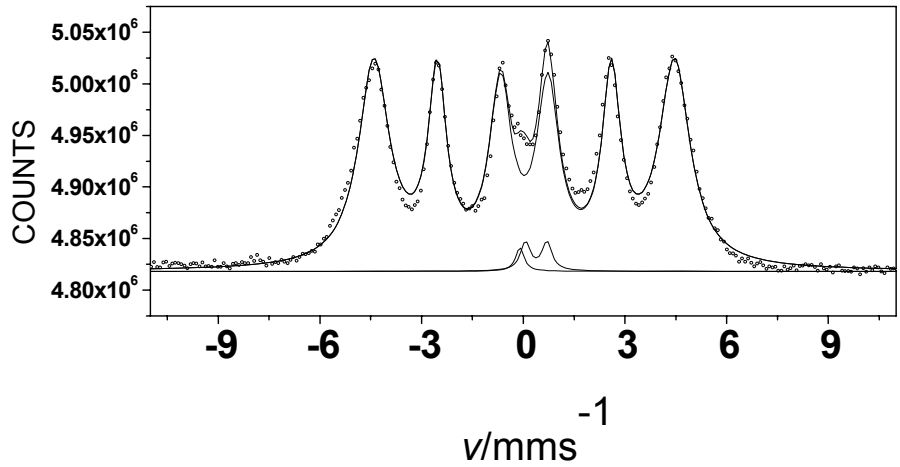

Fig. 2 Mössbauer spectrum of an untreated electrodeposited sample A.

In some cases before the corrosion immersion, an alternate voltage polarization was applied to modify the passive layer to increase in the quantity of iron oxides. The electrode potential was stepped between –0.7 and 0.3 V vs. *sce* for 30 minutes with anodic pulse time 0.2 s and cathodic pulse time 0.1 s (square wave potential cycling (SWPC)).

Following the activation-passivation treatment and the prolonged corrosion, the electrochemical analysis was carried out in fresh solutions. All electrochemical measurements

were carried out on samples that were treated or not treated with SWPC. However, in this study the focus was on the electrochemical characterization of the corrosion layers formed on samples treated with SWPC.

The samples were characterised using the XRD method. The powder diffraction patterns were recorded using a computer controlled powder diffractometer (DRON-2). The measurements were performed with a goniometer set at a speed of 1° cm^{-1}; and β-filtered CoK_α radiation (λ=1.7890), in the range of 2Θ=3–110° at 295K. The powder diffraction patterns were evaluated by an "EXRAY" peak searching computer program (Klencsár, 1998) which gave the cell parameters.

A conversion electron Mössbauer spectra of the electrodeposited alloys and the corroded Fe-Ni-Cr electrodeposits with and without SWPC pre-treatment also were measured with a conventional Mössbauer spectrometer (WISSEL) at room temperature, using a radiating source of 1.85 GBq $^{57}Co(Rh)$. The γ-rays were irradiated perpendicular to the sample plane in a laboratory manufactured gas counter with 2π back scattering geometry, with flowing He + 4% CH_4 gas at 15 cm^3 min^{-1} and applying high voltage at 1200 V. The evaluation of Mössbauer spectra were made by least-square fitting of Lorentzians using the Mosswinn program [16]. The isomer shifts are given relative to α-iron.

3 Results

3.1 XRD and Mössbauer spectroscopic characterization

The broad peaks recorded by the XRD of the electrodeposit at 2θ=52 and 60 degrees (Figure 1) reflects a microcrystalline character, which is similar to those reported earlier for Fe-Ni-Cr alloy coatings electrodeposited under different plating conditions [6].

The Mössbauer spectrum of the deposited sample (Figure 2) is also similar to those reported earlier for Fe-Ni-Cr microcrystalline electroplated alloys [6, 7].

Figure 3 shows the Mössbauer spectra of electrodeposited sample A after completion of the electrochemical treatments.

The Mössbauer spectra of all the figures show the electrodeposits were decomposed into a dominant broad sextet and a small singlet as well as a minor doublet. The Mössbauer parameters of the components are shown in Table 2.

The broad sextet (as an envelop of a number of sextets belonging to the individual Fe microenvironments) is attributed to the highly disordered ferromagnetic Fe-Ni-Cr alloy phase which was identified and reported earlier [6]. The singlet clearly relates to the equilibrium paramagnetic fcc (face centered cubic) phase which was identified during in earlier studies [3, 4]. The doublet is associated with an amorphous ferrihydrite phase, $Fe_5HO_8{\cdot}4H_2O$ as a corrosion product which has been previously reported [17]. A small amount of this phase is even present in the potentiostatically passivated sample. After the potential square wave cycling of samples, the Mössbauer spectra reveal the increase of relative intensity of the doublet related to the ferrihydrite formation. This provides evidence of the formation of a corrosion product on the surface of the electrodeposit. The

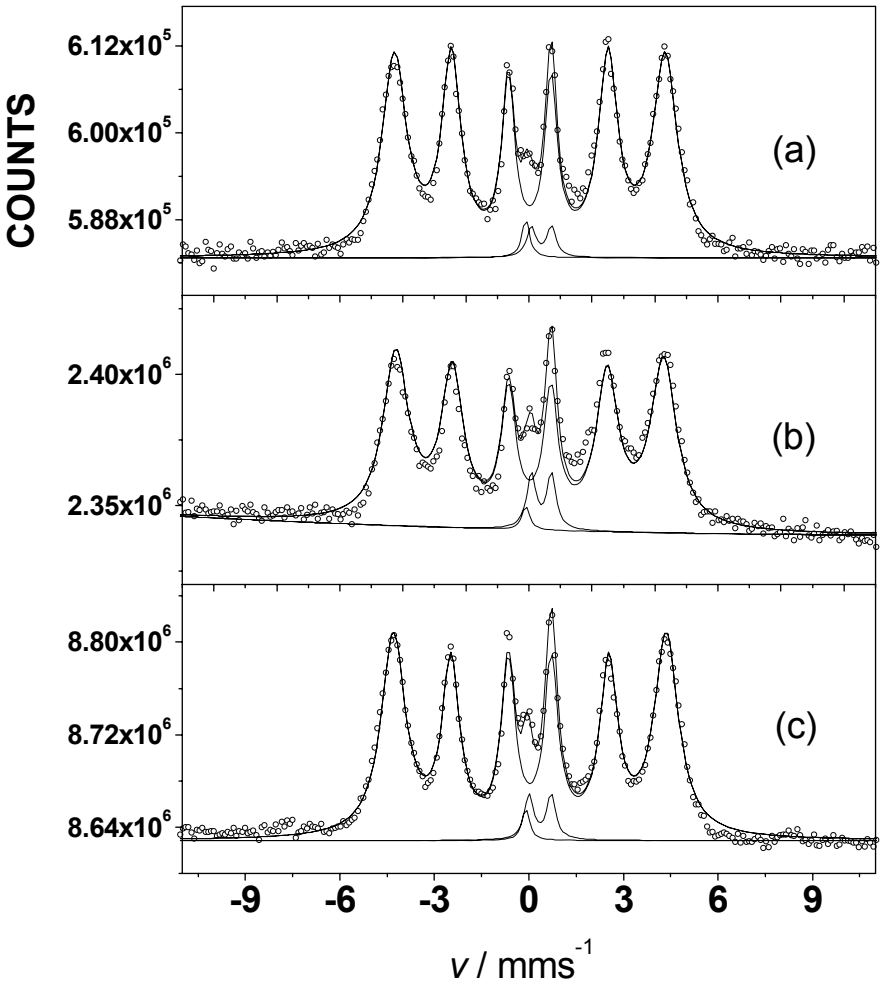

Fig. 3 Mössbauer spectra of electrodeposited sample A: (a) passivated at 0.25 V vs *sce* for 100 minutes; (b) after potential square wave cycling between –0.7 and +0.3 V for 30 minute (duration of the cathodic and anodic pulse was 0.2 and 0.2 s, respectively), and (c) after prolonged corrosion in 0.3 M Na_3BO_3 solution at pH 8.4.

thickness of the corrosion layer on the electrodeposit surface was estimated to be 10 to 15 nanometers, which relates approximately to that calculated from the electrochemical polarization results. Furthermore, it was found that the relative intensity of the 2^{nd} and 5^{th} lines to the 1^{st} and 6^{th} lines, which reflect the magnetic anisotropy, decreases with the corrosion treatments. This clearly demonstrates the effect of the outermost corrosion which gives similar results to that found in earlier work relating to multilayer deposits [18].

Table 2 Mössbauer parameters of electrodeposited and thermally prepared Fe-Ni-Cr samples.

Component	Parameter	electrodeposited sample A	electrodeposited sample A passivated at 0.25 V vs sce for 100 minutes	electrodeposited sample A after potential square wave cycling between –0.7 and +0.3 V for 30 minute	electrodeposited sample A after prolonged corrosion in 0.3 M Na_3BO_3 solution at pH 8.4
Sextet	δ/mms^{-1}	0.029 ± 0.02	0.023 ± 0.02	0.025 ± 0.02	0.027 ± 0.02
	H/T	27.52 ± 0.6	26.56 ± 0.6	26.36± 0.6	26.86± 0.6
	A/%	97.25 ± 0.4	96.2 ± 0.4	94.0 ± 0.5	95.1 ± 0.5
Doublet	δ/mms^{-1}	0.38 ± 0.03	0.39 ± 0.03	0.39± 0.03	0.35± 0.04
	Δ/mms^{-1}	0.63 ± 0.03	0.64 ± 0.03	0.64 ± 0.03	0.69± 0.04
	A/%	2.0 ± 0.15	2.7 ± 0.2	5.1 ± 0.25	3.8± 0.2
Singlet	δ/mms^{-1}	–0.10 ± 0.02	–0.10 ± 0.02	–0.10 ± 0.02	–0.10 ±0.02
	A/%	0.72 ± 0.22	1.1 ± 0.3	0.9 ± 0.2	1.1 ± 0.25

3.2 Electrochemical characterization

3.2.1 Potentiodynamic, chronopotentiometric polarization, and square wave potential cycling measurements

Figure 4 shows typical potentiodynamic polarization curves in 0.3 mol dm^{-3} Na_3BO_3 solution of pH 8.4 recorded with a high scan rate of 0.1 V s^{-1}.

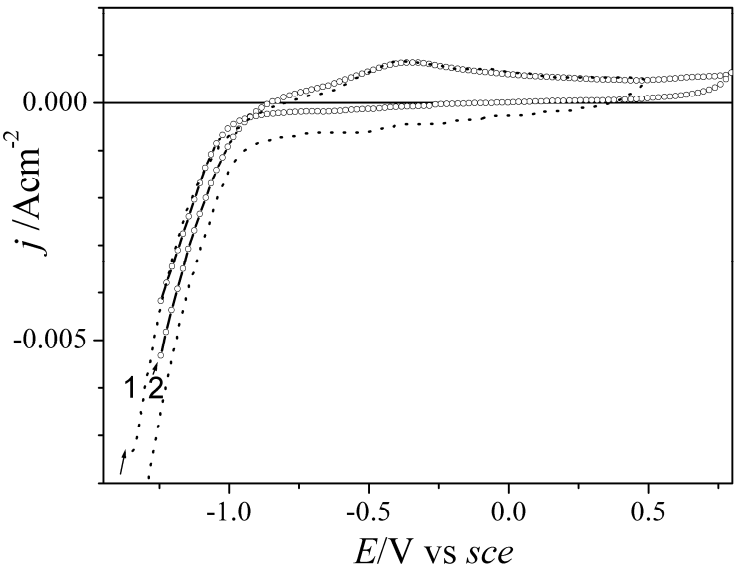

Fig. 4 Cathodic-anodic potentiodynamic curves of the $Fe_{29}Ni_{51}Cr_{20}$ alloy electrodeposits: 1 – sample A, 2 – sample B. Scan rate 0.1 Vs^{-1}.

Figure 4 also shows one broad anodic current peak present at approximately –0.37 V. Close to the zero current potential on the potentiodynamic curves, the chromium dissolution/passivation occurs and the continued current increase above –0.7 V is due to the iron dissolution. Previous studies by Carmezin et al. have also supported these findings [19]. On this basis, a passivating pretreatment was performed with square wave potential cycling between –0.7 V cathodic and 0.3 V anodic potentials. A rapid passivation of the electrodeposited Fe-Ni-Cr alloys can be observed during the potential cycling passivation treatment. Figure 5 shows the switching of the electrode potential of an activated sample from –0.7 V to 0.3 V corresponding to the passive range results in the anodic current decaying to almost zero within 0.2 s.

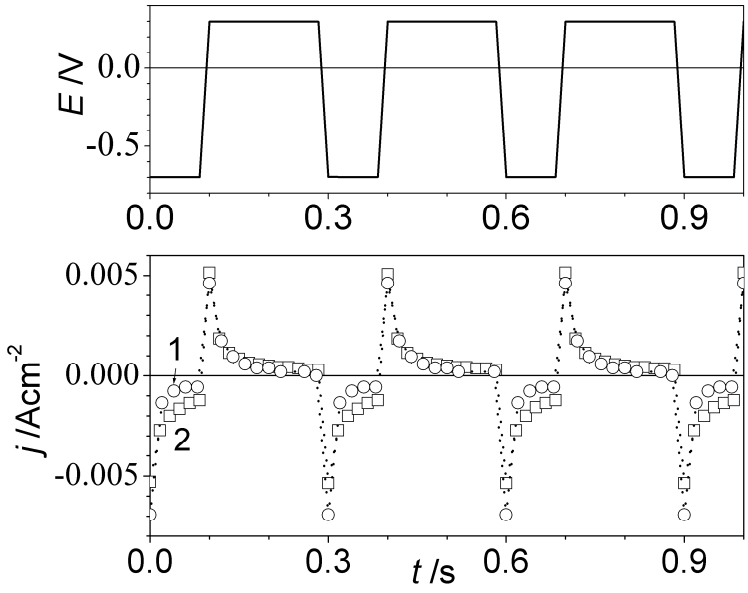

Fig. 5 The input square wave potential versus time, and the resulting current versus time curves: for the $Fe_{29}Ni_{51}Cr_{20}$ electrodeposit 1–A, and 2–B sample.

During the square wave potential cycling passivation, the reactions are expected at –0.7 V and involve the partial reduction of the higher valencey oxides to lower valence states. However, this potential is not low enough to result in the reduction of the chromium oxides within the barrier layer. At 0.3 V, the transient anodic current mainly results from the iron dissolution/passivation, and oxidation of the adsorbed Fe(II)-hydroxides to hydrated Fe(III)-oxides, and this results in an increase in the volume of the deposited part of the passive film which agrees with earlier published work [20, 21].

The stability of the corrosion layers formed on electrodeposited alloys was investigated with chronopotentiometric measurements at different reduction currents. Figure 6a shows a typical potential decay curve for the SWPC treated sample previously immersed in the de-aerated borate solution of pH 8.4 for 18 h.

The reduction behaviour of the corrosion passive films resulted in two potential arrests. The Cr-containing oxides cannot be characterized using galvanostatic cathodic reduction as the arrests relate to the partial reduction of hydrous iron oxides. The potential arrests

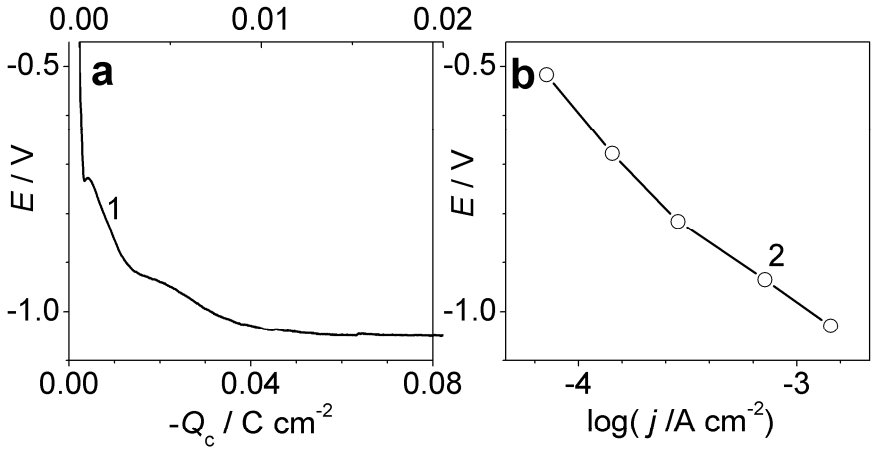

Fig. 6 (a) Potential decay curve following a –0.07 mA cm^{-2} current step from the corrosion potential: for $Fe_{29}Ni_{51}Cr_{20}$ electrodeposit 1–A sample after 18 h immersion time following a SWPC treatment, and (b) steady-state reduction curve constructed from current step potential decay traces after 18 h immersion time, 2–B sample.

at –0.73 and –0.93 V were attributed to the reduction of hydrated Fe_2O_3 and Fe_3O_4 to soluble Fe^{2+}, respectively, which is in agreement with earlier results reported by Bardwell et al. [22]. The estimated thickness of the more easily reduced part of the passive layer was found to be approximately 14 nm.

Figure 6b illustrates that the steady-state cathodic curve constructed from current step potential–time traces are associated with the significant reduction current of the oxide reduction/hydrogen evolution for the electrodeposited Fe-Ni-Cr alloy. This can also be seen from the backward scans of the potentiodynamic curves in Figure 4.

3.2.2 Electrochemical impedance spectroscopic measurements

EIS was used to obtain a detailed characterization of the metal dissolution in passive state. The impedance spectra were recorded in potentiostatic mode at the corrosion potential of the $Fe_{29}Ni_{51}Cr_{20}$ electrodeposits after various passivation/corrosion treatments.

It has been well documented that the transfer function of a highly blocked, electronically conductive barrier layer is expected to be capacitive (i.e. vertical line in the complex impedance Z plane as in case of an ideally polarizable surface [23]). However, it becomes essentially resistive (semicircle in the Z plot) if the dissolution/growing of the passive film and cathodic reaction occur through the layer and at the oxide-solution interface. It has also been reported that the processes of passive dissolution at the anodic potential are governed by the electrical and mass transport properties of the passive layer [24–27]. However, at the mixed potential, the corrosion processes at the oxide/solution interface also need to be further investigated.

The impedance diagrams which are plotted on the complex impedance plane and the Bode plots for the different corrosion layers of the electrodeposited A and B samples, respectively, are shown in Figures 7 and 8.

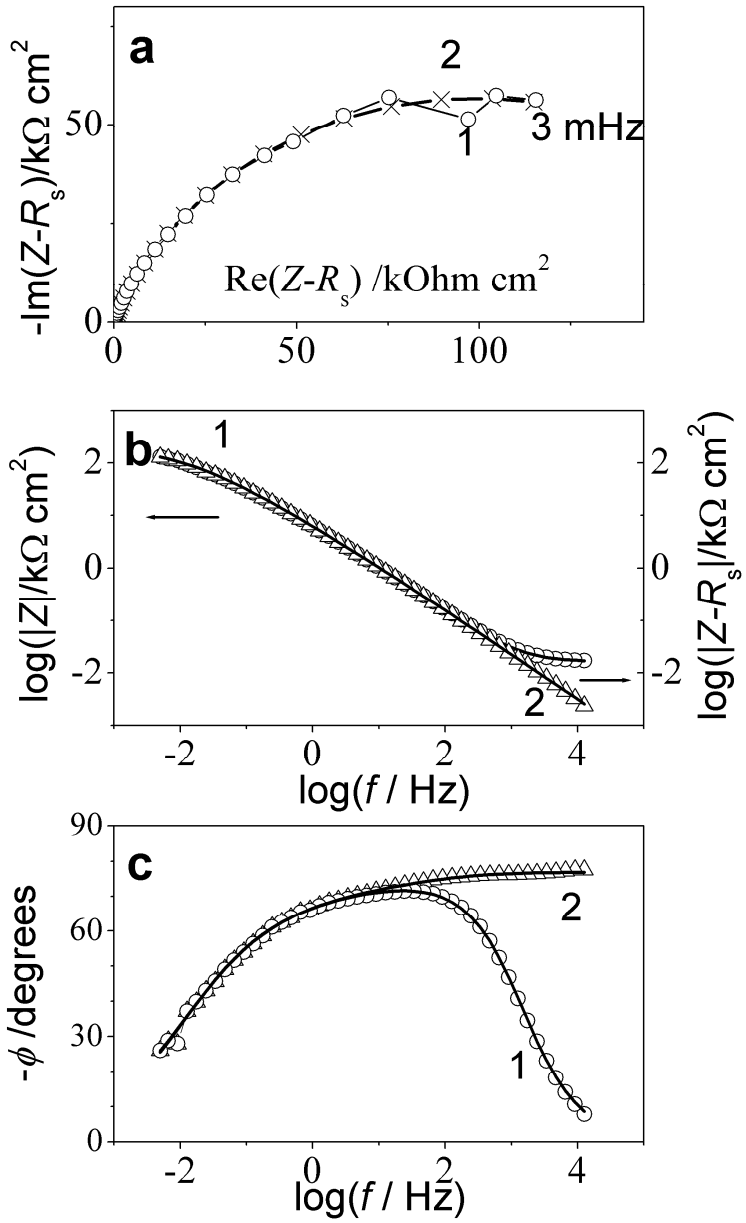

Fig. 7 Measured and calculated (according to the EC model of Fig. 9a.) impedance diagrams determined at the corrosion potential E_{corr} = –0.086 V of the electrodeposited sample A after 18 h corrosion immersion followed the SWPC treatment: (a) in complex plane: 1-o- measured, 2-x- fitted data; (b) and (c) the corresponding Bode plots: 1, 2 – with symbols the measured, with solid lines the fitted data; 1- original data, 2 – 1 data set with subtraction of solution resistance.

The complex plane impedances shown in Figures 7a and 8a do not show definite semicircle-like arcs, therefore exact values of the steady-state polarization resistances ($R_p = |\ \mathrm{Z(j\omega)}|_{\omega\to 0} - |\ \mathrm{Z(j\omega)}|_{\omega\to\infty}$) cannot be estimated by graphical extrapolation. The low frequency impedance limit can be observed from the Bode plots shown as curve 1 in Figures 7b and 8c. The magnitudes of the impedance at low frequency do not differ

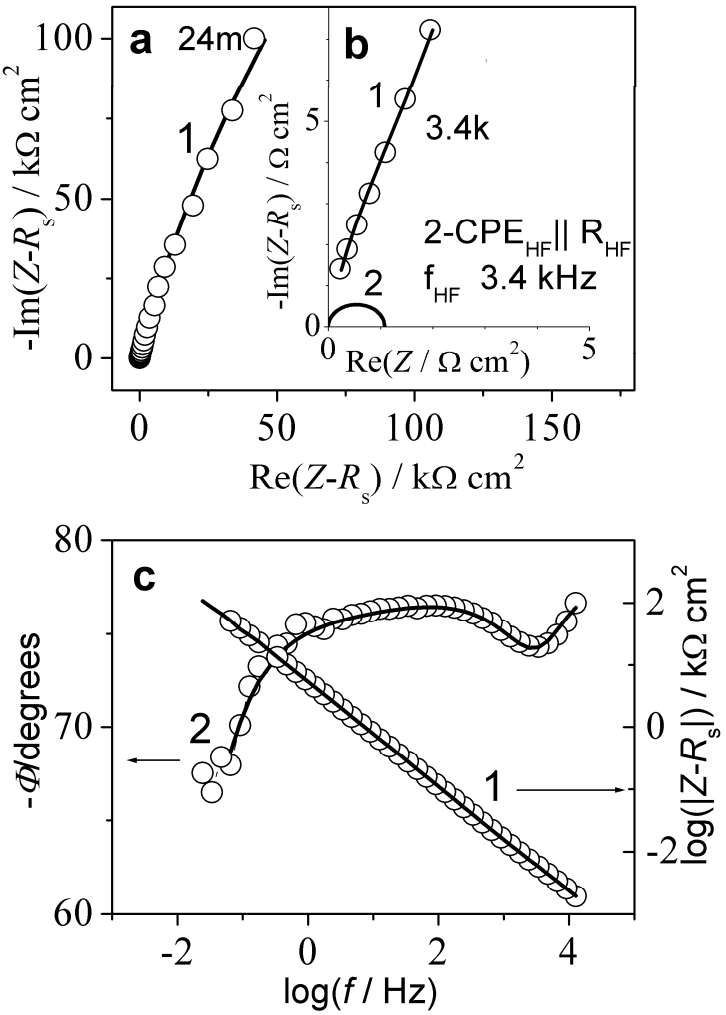

Fig. 8 Measured and calculated (according to the EC model of Fig. 9b.) impedance diagrams determined at the corrosion potential E_{corr} = –0.312 V of the electrodeposited sample B after 18 h wet immersion and 18 h atmospheric corrosion followed the SWPC treatment: (a) in complex plane 1-o- measured, solid line- fitted data; inset (b) 1 – HF part and 2 – calculated HF CPE||R sub-circuit of EC model on Fig. 9b; (c) the corresponding Bode plots 1, 2-o- measured, solid lines- fitted data, 1 – original data, 2 – 1 data set with subtraction of solution resistance.

markedly for the corrosion films formed under de-aerated and aerated conditions. However, for the corrosion film formed in air, the LF slope of the log|Z|-log$f$ curve is markedly higher than 0, therefore, showing capacitive behaviour of the passive layer due to a slow charge transfer "leakage" reaction at the electrode/solution interface.

An analysis of the impedance diagrams from Figures 7 and 8 reveal that the impedance data are composed of distributed or overlapping time constants of parallel R||C or R||CPE circuits (except for the solution resistance-high frequency capacitance). The phase angle-frequency curves calculated from the data after subtracting the solution resistance clearly

indicate (cf. curves 2 on Figures 7c and 8c) a high frequency (3.4 kHz) time constant for the air-corroded B sample. The equivalent circuits (ECs) proposed to fit the impedance diagrams shown in Figures 7 and 8 are shown in Figures 9a and 9b for both samples A and B, respectively.

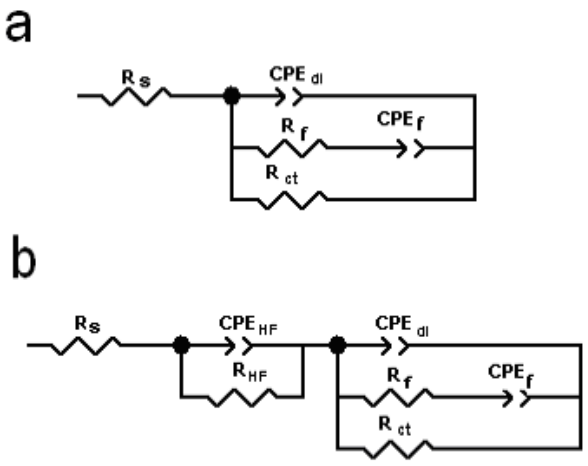

Fig. 9 Equivalent circuits corresponding to the CNLS calculation of impedance spectra of Figure 7 and 8: (a) Fe-Ni-Cr electrodeposit, sample A after 18 h corrosion at E_{corr} = –0.086 V (b) Fe-Ni-Cr electrodeposit, sample B after 18 h wet and 18 h dry corrosion cycle followed the SWPC treatment, at E_{corr} = –0.312 V. The physical meanings of the elements are described in the text.

An examination of Figures 7a-8a shows that the physical interpretation of the ECs can be based on the correlation of the interfacial corrosion reactions and the electronic properties of the passive film. The equivalent circuit presented in Figure 9a is interpreted in the following manner: the solution resistance is connected in series with an MF-LF sub circuit. This CPE||R-CPE||R circuit represents the description of the processes at the passive film/solution interface.

Literature reports that the passive film for austenitic stainless steels can be best described as a duplex structure [19, 28]. In neutral/alkaline solutions the outer part of the film consists mainly of hydrated trivalent iron and chromium oxides, whereas the inner part of the film consists of an anhydrous Cr enriched Fe-Cr oxide. The first parallel CPE||R sub-circuit of Figure 9b can be formally ascribed to the conductivity of the inner semiconductive barrier layer while the second parallel CPE||R-CPE||R sub-circuit can be attributed to the outer layer|solution polarization.

At the corrosion potential ($\sim \pm$ 0.1 V) the oxide layer of an Fe-Ni-Cr alloy can be characterized as a non-stiochiometric, n-type semiconductive oxide in which the electron donor defects are partially or fully ionized and due to this, the space charge layer in the film is in the depleted state ($U_{flatband}$= –0.5 V [19, 29, 30]). The upward bending of the conduction band energy relative to the Fermi level gives rise to a potential drop in the space charge layer which hinders the anodic half reaction. Therefore the anodic reaction is governed by electron and transport properties of the passive layer. Taking into ac-

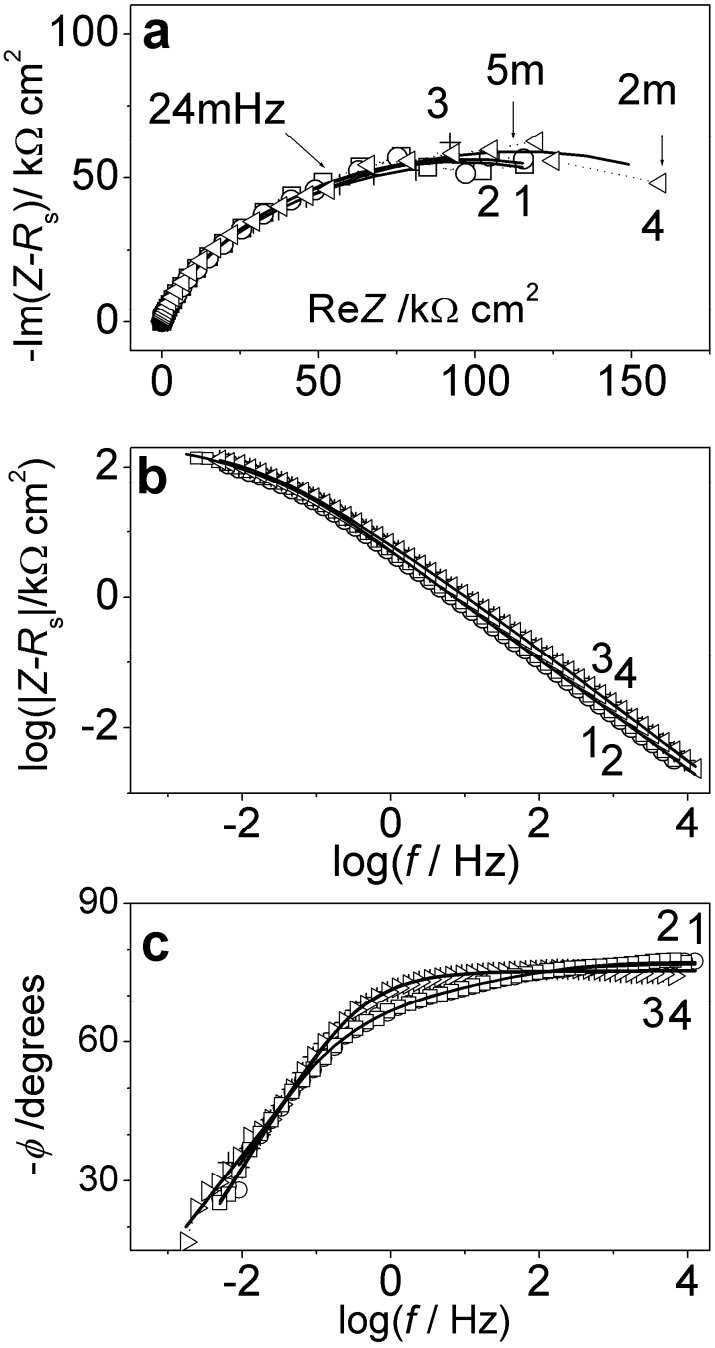

Fig. 10 Measured and calculated (according to the EC model of Fig. 9a.) impedance diagrams determined at the corrosion potentials of two parallel electrodeposited samples after 18 h corrosion immersion followed the SWPC treatment: 1,2 and 3,4 are the successively measured spectra of each sample, respectively. E_{corr} values were: 1-o- –0.086 V; 2-x- –0.089 V; 3- +− –0.296 V; 4-∇ - –0.299 V. (a) in complex plane: 1-4 measured, solid line- fitted data; (b) and (c) the corresponding Bode plots: 1-4 –with symbols the measured, with solid lines the fitted data;

count the point defect model described in the literature by Macdonald et al. [24, 25] and modified by Bojinov et al. [26, 27] for the description of the passive dissolution of the anodically formed passive films of Fe-Cr and Ni-Cr alloys, the transport of interstitials or vacancies[¶] involves the outward movement of the cation defects (mainly Fe_i^{2+} in the interstitial positions and the outward movement of oxide ion defects ($V_{O^{2+}}$) which supply the O^{2-}ions from water at the film/solution interface for the film dissolution and growth. If the film/solution interface is impermeable to the charge carriers, then the diffusion of an electroactive species in the film can be represented by a finite-length diffusion impedance element with a reflective boundary condition which has been previously reported [24, 32]. The restrictive finite-length diffusion impedance can be expressed by the expression as $W_F = \sigma_W(\mathrm{j}\omega)^{-0.5}\coth(\mathrm{j}\,\tau_d\omega)^{0.5}$ where the diffusion time constant is defined as $\tau_d = d^2/\,D$ (d – film thickness , D – diffusion coefficient), and $\sigma_W$is the Warburg parameter. It is known that at the LF limit the W_F reduces to a series R_{LF}-C_{LF} circuit where the $C_{LF} = (\tau_{\,d})^{0.5}/\,\sigma_W$ frequency independent redox capacitance dominates the resultant capacitive behaviour. An examination of the impedance diagrams reveals that the transport of mobile defects is probably not the rate determining step at as low a frequency as 5 mHz because the blocking (capacitive) behaviour is absent at the LF part. Therefore, in the de-aerated solution, where the O_2 concentration is very low, it can be assumed that the cathodic reaction is charge transfer controlled. The transfer resistances R_{ct} of ECs shown in Figure 9 can be assigned to the impedance of the interfacial cathodic reaction. The rate determining step of anodic reaction which likely involves the oxidative dissolution of the Fe_i^{2+} at the oxide/solution interface can be accounted formally with the R-W_{INF} charge transfer resistance-Warburg diffusion impedance connected in series according to a mixed, charge transfer and diffusion controlled kinetics. If the concentration wave caused by the disturbed diffusion process at the lowest frequency does not penetrate through the entire thickness of the diffusion layer, i.e. the $(D/\omega)^{0.5}\langle\langle d$ relation holds, then the infinite-length diffusion impedance describes the mass transport process, $W_{INF} = Y^{-1}(\mathrm{j}\omega)^{-0.5}$, where Y^{-1} is usually denoted as Warburg parameter σ_W Ohm·cm^2·s$^{-0.5}$.As the complex non-linear-least-squares curve fitting for the impedance data of the corroding electrodeposits CNLS gives a better weighted sum of squares as a good fit, if a restrictive finite-length Warburg impedance [32] (the concentration wave is blocked at the metal/film interface) substitutes the infinite length Warburg impedance, it can therefore be deduced that the diffusion process is occurring in the film-side of the interface. However, in order to get a better idea of the nature of passive dissolution reactions on the electrodeposited alloy further investigations is required.

It is well known that the non-ideal capacitive impedance elements accounting for the double layer charging or other ionic movements can be formally described with a constant phase element (CPE) as $Z_{CPE} = Y^{-1}(\mathrm{j}\omega)^{-n}$. Clearly, if n=1 then Y has the meaning of a capacitance in F cm^{-2}. If the value of exponent n is between 0.5–1 then Z_{CPE}

[¶] According to the notation proposed by Kröger and Vink [31] the typical defects in a spinel-type lattice of iron-oxide passive films [26]: Fe_i^{2+} – interstitial iron (II) cation in octahedral, $V_{Fe^{3-}}$ – triple negative iron ion vacancy in tetrahedral positions, and $V_{O^{2+}}$ – doubly positive oxygen vacancy.

can be related to a non-ideal double layer capacitance with distributed coupling of the double layer capacitance of a rough or porous surface with the electrolyte resistance, or in the case of passive films, it has been shown [23, 33] in the literature that the constant phase behaviour can be caused by the inhomogeneity of conductivity in the depth of the film. For the electrodeposits corroded either in a de-aerated solution or exposed to air, the calculated Y_{CPE} parameter in Table 3 gives a reasonable value for the double layer capacitance on an inhomogeneous oxide covered surface, from which according to the $C = Y(\omega^*)^{n-1}$ relation [34] a 15.5 or 14.8 μF·cm^{-2} double layer capacitance can be calculated.

Table 3 Parameters used to fit the EIS spectra of $Fe_{29}Ni_{51}Cr_{20}$ electrodeposited alloys corresponding to the models of Figure 9 between 17 KHz and 24 mHz frequency range[1].

Parameters of impedance spectra on Figs. 7-8	$Fe_{29}Ni_{51}Cr_{20}$ electrodeposit A		$Fe_{29}Ni_{51}Cr_{20}$ electrodeposit B	
	Mean value	Error %	Mean value	Error %
R_s/ Ω	32.6	0.3	23.6	0.8
$Y_{CPE\text{-}HF}$/ μF·cm^{-2}·s^{n-1}			40.9	28.1
n_{HF}			1	fixed
R_{HF}/ Ω·cm^2			1.1	33.5
$Y_{CPE\text{-}dl}$/ μF·cm^{-2}·s^{n-1}	25.3	0.3	25.8	16.2
n_{dl}	0.85	0.4	0.90	2.1
C_{dl}/ μF·cm^{-2}	15.5		14.8	
R_f/ kΩ·cm^2	2.5	39.7	0.3	50.2
$Y_{CPE\text{-}f}$/ μF·cm-2·s^{n-1}	17.7	3.6	14.8	28.5
n_f	0.52	1.5	0.69	3.3
R_{ct}/ kΩ·cm^2	208.3	2.4	893.7	8.8
Weighted sum of squares of fit	0.0035		0.0072	
Degree of freedom	38		36	
Standard error %	1.0		1.4	

[1] Sample A was corroded in de-aerated borate solution for 18 h, sample B was exposed to air for 18 h following the 18 h wet corrosion. Measurements were carried out in de-aerated borate solution at pH 8.4.

The phase shift vs. frequency plot (curve 2) in Figures 7c and 8c reveal that at the high frequency part of the diagram there is no sign of an HF time constant for the electrodeposited alloy corroded in de-aerated solution compared with the corroded alloy in an aerated condition. This may be due to the absence of Cr-rich barrier layer in the passive film. For the air corroded samples the simulation of the HF CPE|| R sub-circuit can also be seen in the b inset of the Figure 8 (curve 2). The structural models proposed for the impedance spectra reveal the formation of an inner barrier layer and a hydrous part of the passive film on the air-corroded electrodeposit. Similar results have already been reported with stainless steel [19, 28]. For the electrodeposited alloy corroded in de-aerated solution it can be assumed that a thinner layer of Fe-rich passive film exists where

the rate of the cathodic process is significant. As a consequence of this, the corrosion rate is inversely proportional to R_{ct} (Table 3). In the passive state this is approximately five times lower for the electrodeposited alloy corroded in aerated conditions compared to the alloy corroded in the de-aerated solution.

The satisfactory standard errors of the fit in Table 3 show the validity of our impedance evaluations. However, it is known that EIS is a very sensitive tool to characterize the instantaneous surface state of the corroding specimen. Even in case of a steady-state corrosion process, the LF impedance data may be distorted caused either by the slow drift in time or the interfacial parameters may be different on parallel samples due to different roughness, porosity or incidental change in composition. We have investigated the reproducibility of the impedance spectra measured under the same corrosion conditions on different $Fe_{29}Ni_{51}Cr_{20}$ samples and successively on the same sample.

Fig. 10 is a good reproduction of an EIS spectra as demonstrated by the measured data of the corroded samples in de-aerated borate solution for 18 h, as well, all data-sets could have been fitted to the same EC model of Fig. 9a. Similar observations were also gained on the parallel air-corroded samples. The standard errors of the fits varied between 0.6–2.2 % for each system. Based on the standard errors of the R_{ct} values of Table 4 we can consider that the air-formed passive films exhibit significantly higher corrosion stability than that formed during corrosion in de-aerated solution.

Further investigation may reveal whether the ability of the electrodeposited Fe-Ni-Cr alloy offers protection against non-uniform pitting corrosion as has been observed for other amorphous/microcrystalline materials recorded in the literature [8, 11].

Table 4 Reproducibility of the fitted charge-transfer resistances of the corrosion process of $Fe_{29}Ni_{51}Cr_{20}$ electrodeposits.

	R_{ct} / kΩ·cm^2	
	2 parallel samples were corroded in de-aerated borate solution for 18h[2]	2 parallel samples were exposed to air for 18 h following the 18 h wet corrosion[3]
Mean value	220.2	1016.2
Standard error %	4.1	6.0

[2] number of parallel measurements was 4
[3] number of parallel measurements was 3

In the literature, research illustrates the structure-property relationship of electrodeposited iron based alloys of various compositions produced with different deposition variables [35, 36]. A number of alloys of amorphous-nanocrystalline structure have been reported to exhibit good corrosion resistance compared to other variants. In our work, we have given a detailed electrochemical characterization of the complex corrosion films existing on the amorphous $Fe_{29}Ni_{51}Cr_{20}$ alloy electrodeposited from trivalent chromium dimethylformamide-water electrolytes.

4 Conclusions

The high charge transfer resistance values obtained by the CNLS fitting of the impedance data reveal the stability of the corrosion films of the $Fe_{29}Ni_{51}Cr_{20}$ alloy in borate solution.

The structural models derived from the impedance spectra confirmed the presence of an inner barrier within the passive film on the electrodeposited Fe-Ni-Cr alloy corroded under aerated conditions.

Mössbauer spectroscopic results support the formation of a Fe rich passive film (mainly ferrihydrite) in the electrodeposits, the amount of this can be increased by the cathodic to anodic potential cycling passivation procedure.

Acknowledgement

Financial support from the Hungarian National Science Fund (T043687, T68135 and M042115) is gratefully acknowledged.

References

[1] J.R. Thompson, A. Goyal, D.K. Christen and D.M. Kroeger: "Ni-Cr textured substrates with reduced ferromagnetism for coated conductor application", *Physica C*, Vol. 370, (2002), pp. 169–176.

[2] A. Vértes, L. Korecz and K. Burger: *Mössbauer Spectroscopy*, Elsevier, Amsterdam, 1979.

[3] E. Kuzmann, S. Stichleutner, M. El-Sharif, C.U. Chisholm, L. Sziráki and A. Vértes: "Mössbauer Investigation of Electrodeposited Sn-Zn, Sn-Cr, Sn-Cr-Zn and Fe-Ni-Cr Coating", *Hyp. Int.*, Vol. 141, (2002), pp. 425–433.

[4] E. Kuzmann, M. El-Sharif, C.U. Chisholm, G. Principi, C. Tosello, A. Gupta, K. Havancsák, L. Takács and A. Vértes: "Mössbauer Studies of Electrodeposited and Ion Beam Mixed Alloy Coating", *Hyp. Int.*, Vol. 139–140, (2002), pp. 193–204.

[5] M.R. El-Sharif, A. Watson and C.U. Chisholm: "The sustained deposition of thick coatings of chromium/nickel and chromium/nickel/iron alloys and their properties", *Trans IMF*, Vol. 66, (1988), p. 34.

[6] E. Kuzmann, M.R. El-Sharif, C.U. Chisholm and A. Vértes: "Conversion electron Mössbauer study of short range ordering in electrochemically deposited Fe-Ni-Cr alloy", *J. Radioanal. and Nucl. Chem.*, Vol. 190, (1995), pp. 327–332.

[7] L. Sziráki, E. Kuzmann, M.R. EL-Sharif, C.U. Chisholm, G. Principi, C. Tosello and A. Vértes: "Electrochemical behaviour of electrodeposited strongly disordered Fe-Ni-Cr alloy", *Electrochem. Commun.*, Vol. 2, (2000), pp. 619–625.

[8] U. Erb, K.T. Aust and G. Palumbo: "Electrodeposited nanocrystalline materials", In: C.C. Koch (Ed.): *NanoStruct Mater.*, Noyes publications/W. Andrew Publ., Norwich, 2002, Ch. 5.

[9] M.I. Kjuchukova, S.D. Vitkova, O.L. Blagiev, V.V. Ivanova and G.M. Raichevski:

"X-ray photoelectron spectroscopic studies of the anodic behaviour of amorphous chromium-carbon and crystalline chromium electrodeposits", *Bulgarian Chem. Commun.*, Vol. 31, (1999), pp. 25–37.

[10] U. Erb: "Electrodeposited nanocrystals: synthesis, properties and industrial application", *NanoStruct. Mater.*, Vol. 6, (1995), pp. 533–438.

[11] B. Inturik and Z. Szklarska-Smialowska: "Localised corrosion of nanocrystalline 304 type stainless steel films", *Corrosion*, Vol. 48, (1992), pp. 398–400.

[12] L. Kwiatkowski and F. Mansfeld: "Surface modification of stainless steel by an alternating voltage process", *J. Electrochem Soc.*, Vol. 140, (1993), pp. L39–L41.

[13] S. Fujimoto, K. Tsujino K. Wada and T. Tsutae: "Electrochemical conditions for coloured film formation on type 304 stainless steel with square wave polarization", *Corros. Sci.*, Vol. 35, (1993), pp. 147–152.

[14] S. Fujimoto, K. Tsujino and T. Shibata: "Growth and properties of Cr-rich thick and porous oxide films on Type 304 stainless steel formed by square wave potential pulse polarisation", *Electrochim. Acta*, Vol. 47, (2001), pp. 543–551.

[15] M. Vukovic : "Formation and growth of hydrous oxide film on stainless steel in alkaline solution by potential cycling", *Corros. Sci.*, Vol. 37, (1995), pp. 111–120.

[16] Z. Klencsár, E. Kuzmann and A. Vértes: "User-friendly software for Mössbauer spectrum analysis", *J. Radioanal. Nucl. Chem.*, Vol. 210, (1996), pp. 105–118.

[17] E. Murad and J.H. Johnston: "Iron Oxides and Oxyhydroxides", In: G.J. Long (Ed.): *Mössbauer Spectroscopy Applied to Inorganic Chemistry*, Vol. 2, Plenum Press, New York, 1987, p. 533.

[18] A. Vértes, Gy. Vankó, Z. Németh, Z. Klencsár, E. Kuzmann, Z. Homonnay, F.H. Kármán, E. Szücs and E. Kálmán: "Nanostructure of vapor-deposited ^{57}Fe thin films", *Langmuir*, Vol. 18, (2002), pp. 1206–1210.

[19] M.J. Carmezin, A.M. Simões, M.F. Montemor and M. Da Cunha Belo: "Capacitance behaviour of passive films on ferritic and austenitic stainless steel", *Corr. Sci.*, Vol. 47, (2005), pp. 581–591.

[20] N. Sato and G. Okamoto: "Passivity of metals", In: J. O'Bockris (Ed.): *Comprehensive Treatise of Electrochemistry*, Vol. 4, Plenum Press, NY, 1981, Ch. 4.

[21] D.C. Agarwal: "Nickel and nickel alloys", In: R.W. Revie (Ed): *Uhlig's Corrosion Handbook*, J. Wiley & Sons, Inc., New York, 2000, Ch. 45.

[22] J.A. Bardwell, G.I. Sproule, D.F. Mitchell, B. Macdougall and J. Graham: "Nature of the passive film on Fe-Cr alloys as studied by 18O secondary mass spectrometry: reduction of the prior film and stability to ex-situ surface analysis", *J. Chem. Soc. Faraday Trans.*, Vol. 87, (1991), pp. 1011–1019.

[23] Z. Stoynov and D. Vladikova: *Differential Impedance Analysis*, M. Drinov Akad. Publ. H., Sofia, 2005, p. 46.

[24] D.D. Macdonald: "Point defect model for the passive state", *J. Electrochem. Soc.*, Vol. 139, (1992), pp. 3434–3449.

[25] D.D. Macdonald: "Passivity-the key is our metals-based civilization", *Pure Appl. Chem.*, Vol. 71, (1999), pp. 951–978.

[26] M. Bojinov, G. Fabricius, T. Laitinen, K. Mäkelä, T. Saario and G. Sundholm: "Coupling between ionic defect structure and electronic conduction in passive films on iron, chromium and iron-chromium alloys", *Electrochim. Acta*, Vol. 45, (2000), pp. 2029–2048.

[27] M. Bojinov, G. Fabricius, P. Kinnunen, T. Laitinen, K. Mäkelä, T. Saario and G. Sundholm: "Electrochemical Study of the passive behaviour of Ni-Cr alloys in a borate solution-a mixed-conduction model approach", *J. Electroanal. Chem.*, Vol. 504, (2001), pp. 29–44.

[28] C.R. Clayton and I. Olefjord: "Passivity of austenitic stainless steels", In: P. Marcus and J. Oudar (Eds.): *Corrosion mechanism in theory and practice*, Marcel Dekker, NY, 1995, Ch. 6.

[29] G. Goodlet, S. Faty, S. Cardoso, P.P. Freitas, A.M. Simões, M.G.S. Ferreira and M. Da Cunha Belo: "The electronic properties of sputtered chromium and iron oxide films", *Corr. Sci.*, Vol. 46, (2004), pp. 1479–1499.

[30] S.R. Morrison: *Electrochemistry at semiconductor and oxidized metal electrodes*, Plenum Press, NY, 1980, Ch. 5.

[31] F.A. Kröger: *The Chemistry of Imperfect Crystals*, Vol. 2, North-Holland Publishing, Amsterdam, 1974, p. 31, 744.

[32] I.D. Raistrick, D.R. Franceschetti and J.R. MacDonald: "Theory", In: J. Barsoukov and J.R. MacDonald (Eds): *Impedance spectroscopy: Theory, experiments, and applications*, Wiley-Interscience, N.J., 2005, Ch. 2.

[33] C.A. Schiller and W. Strunz: "The evaluation of experimental dielectric data of barrier coatings by means of different models", *Electrochim. Acta*, Vol. 46, (2001), pp. 3619–3625.

[34] C.H. Hsu and F. Mansfeld: "Concerning the conversion of the constant phase element parameter Y_0 into a capacitance", *Corrosion*, Vol. 57, (2001), pp. 747–748.

[35] N.V. Myunk and K. Nobe: "Electrodeposited Iron Group Thin-Film Alloys: Structure-Property Relationships", *J. Electrochem. Soc.*, Vol. 148, (2001), pp. C136–C144.

[36] Sh. Deng and Z. Gong: "The electrochemical behaviour of pulse-plated nanocrystalline iron-nickel-chromium alloy", *Anti-Corrosion Methods and Materials*, Vol. 50, (2003), pp. 267–270.